Journal of Sound and Vibration 329 (2010) 2497–2515

Contents lists available at ScienceDirect

Journal of Sound and Vibration

journal homepage: www.elsevier.com/locate/jsvi

Energy harvesting under excitations of time-varying frequency

Thiago Seuaciuc-Osório, Mohammed F. Daqaq *

Nonlinear Vibrations and Energy Harvesting Laboratory (NoVEHL), Department of Mechanical Engineering, Clemson University, Clemson, SC, USA

ARTICLE INFO

Article history:
Received 22 August 2009
Received in revised form
8 January 2010
Accepted 11 January 2010
Handling Editor: M.P. Cartmell
Available online 6 February 2010

ABSTRACT

The design and optimization of energy harvesters capable of scavenging energy efficiently from realistic environments require a deep understanding of their transduction under non-stationary and random excitations. Otherwise, their small energy outputs can be further decreased lowering their efficiency and rendering many critical and possibly life saving technologies inefficient. As a first step towards this critical understanding, this effort investigates the response of energy harvesters to harmonic excitations of time-varying frequency. Such excitations can be used to represent the behavior of realistic vibratory environments whose frequency varies or drifts with time. Specifically, we consider a piezoelectric stack-type harvester subjected to a harmonic excitation of constant amplitude and a sinusoidally varying frequency. We analyze the response of the harvester in the fixed-frequency scenario then use the Jacobi–Anger's expansion to analyze the response in the time-varying case. We obtain analytical expressions for the harvester's response, output voltage, and power. In-depth analysis of the attained results reveals that the solution to the more complex time-varying frequency can be understood through a process which "samples" the fixed-frequency response curve at a discrete and fixed frequency interval then multiplies the response by proper weights. Extensive discussions addressing the effect of the excitation parameters on the output power is presented leading to some initial suggestions pertinent to the harvester's design and optimization in the sinusoidally varying frequency case.

1. Introduction

Energy harvesting is a process by which otherwise wasted ambient energy can be captured and transformed into a useful form. Historical examples of this concept include windmills, sailing ships, and waterwheels. Modern technologies and current energy needs have brought this same concept to a smaller scale wherein small devices with minute energy consumption can be operated autonomously. This can be achieved by exploiting the ability of some active materials and mechanisms to generate an electric potential in response to mechanical motions or external vibrations [1–3].

Many critical electronic devices, such as health-monitoring sensors [4,5], pace makers [6], spinal stimulators [7], wireless sensors [8–10], etc. require minimal amounts of power to function. Such devices have, for long time, relied on batteries that have not kept pace with the devices' demands, especially in terms of energy density [11]. In light of such challenge, scavenging otherwise wasted energy from mechanical vibrations can provide a solution to lower our dependance on batteries and advance many life-saving technologies.

While most environmental excitations under which energy harvesters are designed to operate do not possess well-defined characteristics and are generally random or have a non-stationary nature in which the frequency or amplitude of

* Corresponding author.
E-mail address: mdaqaq@clemson.edu (M.F. Daqaq).

0022-460X/$ - see front matter © 2010 Elsevier Ltd. All rights reserved.
doi:10.1016/j.jsv.2010.01.015

the excitation vary with time; current research studies have, for the most part, addressed the problem from a steady-state perspective which assumes a harmonic fixed-frequency excitation [12–17]. Two reasons for this assumption lie in the complexities that could arise when one attempts to obtain insightful analytical solutions when the excitation is non-stationary and that most experimental setups are carried in a laboratory environment where the excitation sources can be controlled, and, hence, non-stationarity problems can be avoided.

As of today, it is still not well-understood whether the steady-state fixed-frequency analysis is a good indicator of the harvester's performance in realistic environments or whether one can solely depend on these studies for the design and optimization of energy harvesters. As a first step towards developing this critical understanding, this manuscript delves into the understanding of energy harvester's transduction under a class of harmonic excitations having a time-varying frequency. Such excitations are common especially in rotary machines that vibrate, even in healthy conditions, due to radial magnetic reluctance forces, minute rotational imbalances, and electrical interferences. For instance, turbines, jet engines, generators, and induction motors are usually equipped with a network of sensors to monitor their health condition so as to avoid catastrophic failures and severe economic losses resulting from lengthy shutdowns. These sensors, which usually require minute amount of power to function, are powered through a wiring system that costs more than the sensor itself [18]. In addition to space limitations, the sensor-cable assembly can also cause reliability problems. Such issues can be avoided if these sensors are powered autonomously via energy harvesters that feed on the machines' vibrations. These vibrations are usually harmonic with a frequency that drifts with time and with the machine's rotational speed especially that most rotary machines are currently being equipped with variable-speed drives to ensure maximum efficiency at variable loadings.

In this manuscript, we emphasize frequency profiles having a sinusoidal variation for two reasons. First, such profiles cover both directions of the frequency sweep which permits understanding the effect of the sweep direction on the output power. Second, using a Fourier Series Expansion, other frequency profiles can be transformed into a series of sinusoids which allows us to address more general frequencies by building upon the understanding of the sinusoidally varying frequency case.

The rest of the manuscript is organized as follows: In Section 2, we present the mathematical model of the piezoelectric stack-type harvester under consideration and carry dimensional analysis to identify the important design parameters. In Section 3, we present the response of the harvester to harmonic excitations of a fixed frequency and obtain an approximate analytical solution describing the response of the harvester to sinusoidally varying frequency excitations. We study the convergence of this solution to a numerical integration of the actual equations of motion then use it to obtain an analytical expression for the average power. The availability of these analytical solutions allows us, in Section 4, to perform a parameter study, to understand the influence of the sweep rates and different design parameters on the energy harvesting process. In Section 5, we present some results pertinent to the optimality of the load resistance in the sinusoidally varying frequency case. In Section 6, we make some suggestions with regards to tuning the harvester. Finally, in Section 7, we present our conclusions and recommendation for future work.

2. Mathematical model

We consider a harvester consisting of a piezoelectric (PZT) stack and a proof mass as shown in Fig. 1. The base is subjected to an input excitation, $F(t)$, and the PZT stack is wired to a purely resistive electric load, R_{eq}, through two electrodes. The harvester's governing equations of motion can be expressed as [12]

$$\ddot{x}+2\zeta\omega_n\dot{x}+\omega_n^2 x-\frac{\theta}{m}V=\frac{F_0}{m}\cos(\omega t), \tag{1a}$$

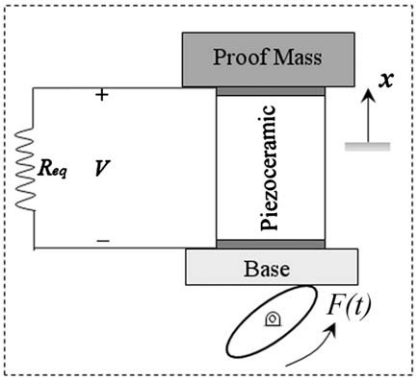

Fig. 1. A schematic of a PZT-stack type energy harvester.

$$\theta\dot{x}+C_p\dot{V}+\frac{1}{R_{\rm eq}}V=0, \tag{1b}$$

$$\omega_n=\sqrt{\frac{K}{m}},\quad m=M+\frac{1}{3}M_p,\quad K=\frac{E_pA_p}{t_p},\quad \theta=-\frac{eA_p}{t_p},\quad C_p=\frac{\varepsilon A_p}{t_p},$$

where ζ is the mechanical damping ratio, ω_n is the natural frequency of the mechanical system, K is the effective stiffness of the PZT stack, A_p and t_p are the cross-sectional area and thickness of the PZT, respectively, and E_p is its Young's modulus; m denotes the effective mass of the system which consists of a proof mass, M, and the mass of the piezoelectric stack, M_p. The resistance $R_{\rm eq}=R_LR_p/R_L+R_p$ is the equivalent of the load resistance, R_L, and the piezoelectric resistance, R_p,[1] θ is the effective piezoelectric coupling coefficient, and C_p is the effective capacitance of the piezoelectric stack. The constants e and ε represent, respectively, the piezoelectric constant and electric permittivity of the PZT.

Here, we adopt a linear single-degree-of-freedom (SDOF) model to represent the response because most of the energy harvesting devices considered in the literature have been shown to behave linearly within the operation range of the harvester. The most prolific energy harvesting device, which consists of a piezoelectric cantilevered-type bi-morph, has been extensively modeled in the literature using linear assumptions. Indeed, it has been shown experimentally, see for instance [3,12,13,19,20], that a linear model is sufficient to predict the dynamic behavior of the harvester. With regards to the SDOF assumption, Osorio and Daqaq [21] has shown that, in the case of piezoelectric harvesters, a reduced-order model consisting of a single mode is accurate enough to predict the dynamic behavior provided that the harvester is being excited near that mode.

We consider a harmonic excitation with a fixed amplitude and a sinusoidally varying frequency in the form

$$F(t)=F_0\cos[\omega_ot+b\sin(\omega t)], \tag{2}$$

where ω_o denotes the carrier frequency, ω represents the modulation frequency, and b is the modulation index. When either the modulation index or frequency are set to zero, the instantaneous frequency reduces to ω_o and the excitation $F(t)$ becomes stationary. In simple terms, Eq. (2) represents a forcing function having a frequency which varies sinusoidally around a center value of ω_o with a frequency ω. Since the argument of the cosine in Eq. (2) is the time integral of the frequency, one can also define the instantaneous frequency according to

$$\Omega_{\rm inst}(t)=\omega_o+b\omega\cos(\omega t). \tag{3}$$

2.1. Dimensional analysis

To simplify the system and better understand how different parameters influence the system's response, we perform a dimensional analysis where we introduce the following dimensionless variables:

$$t=\frac{\tau}{\omega_n},\quad x=X\overline{x},\quad V=V_{\rm oc}\overline{V},\quad \omega_o=\Omega_o\omega_n,\quad \omega=\Omega\omega_n, \tag{4}$$

where $X=F_0/K$ represents the maximum displacement and $V_{\rm oc}=\theta X/C_p$ is the open-circuit voltage. Upon substitution of Eq. (4) into Eqs. (1a) and (1b), we obtain

$$\ddot{\overline{x}}+2\zeta\dot{\overline{x}}+\overline{x}-\Theta\overline{V}=\cos[\Omega_o\tau+b\sin(\Omega\tau)], \tag{5a}$$

$$\dot{\overline{x}}+\dot{\overline{V}}+\Gamma\overline{V}=0, \tag{5b}$$

where the derivatives are now with respect to the dimensionless time, τ, and the dimensionless parameters are given by

$$\Theta=\frac{\theta^2}{KC_p},\quad \Gamma=\frac{1}{R_{\rm eq}C_p\omega_n}. \tag{6}$$

Here, Θ represents the effective coupling between the mechanical and electrical subsystems and Γ is the ratio of the mechanical time constant, $1/\omega_n$, and the electrical time constant, $R_{\rm eq}C_p$.

3. Steady-state response

In the case of a fixed-frequency excitation, the steady-state response can be easily obtained as

$$\overline{x}(\tau)=\sqrt{A^2+B^2}\sin\left[\Omega_o\tau+\arctan\left(\frac{A}{B}\right)\right], \tag{7}$$

[1] The piezoelectric resistance is usually orders of magnitude larger than the load resistance, hence the equivalent resistance can be approximated by R_L.

$$\overline{V}(\tau) = \sqrt{C^2+D^2}\sin\left[\Omega_o\tau + \arctan\left(\frac{C}{D}\right)\right], \tag{8}$$

where

$$A(\Omega_o) = \frac{(1-\Omega_o^2)(\Omega_o^2+\Gamma^2)+\Omega_o^2\Theta}{E}, \tag{9}$$

$$B(\Omega_o) = \frac{\Omega_o[2\zeta(\Gamma^2+\Omega_o^2)+\Gamma\Theta]}{E}, \tag{10}$$

$$C(\Omega_o) = \frac{-\Omega_o^2[2\zeta\Gamma+(1-\Omega_o^2)+\Theta]}{E}, \tag{11}$$

$$D(\Omega_o) = \frac{\Omega_o[\Gamma(1-\Omega_o^2)-2\zeta\Omega_o^2]}{E}, \tag{12}$$

and

$$E(\Omega_o) = [(1-\Omega_o^2)^2+4\zeta^2\Omega_o^2](\Omega_o^2+\Gamma^2)+\Theta\Omega_o^2(\Theta+4\zeta\Gamma+2-2\Omega_o^2). \tag{13}$$

After some algebraic manipulations, the amplitude of the voltage developed across the PZT stack can be simplified to

$$\overline{V}_p(\Omega_o) = \frac{\Omega_o}{\sqrt{E(\Omega_o)}}. \tag{14}$$

Using Eq. (14), the amplitude of output power can be expressed as

$$P_p(\Omega_o) = \frac{\overline{V}_p^2(\Omega_o)V_{oc}^2}{R_{eq}}. \tag{15}$$

Fig. 2 depicts the power-response curve in the fixed-frequency case for the numerical values listed in Table 1. In the figure, we normalize the excitation frequency with respect to the non-dimensional resonance frequency of the harvester, Ω_r. The resonance frequency is obtained by solving the eigenvalue problem associated with Eqs. (5a) and (5b) for the parameters listed in Table 1 which yields a resonance frequency of $\Omega_r = 1.1143$. As shown in Fig. 2, we also introduce a measure for the bandwidth of the harvester, Ω_{bw}. In this paper, we define Ω_{bw} as the distance between the resonance frequency and the frequency at which the output power drops below 4 percent of its peak value. For the parameters listed in Table 1, $\Omega_{bw} = 0.2$.

In the sinusoidally varying case, an analytical solution of Eqs. (5a) and (5b) is not easily attainable but is critical to provide valuable insight into the behavior of the system's response in terms of the fixed-frequency power curve and the excitation parameters. What we know about the response of vibratory systems to time-varying excitations dates back to the work of Lewis in 1932 [22] whose studies were later expanded by Cronin [23]. Notably, it was shown that resonance no longer occurs at the system's natural frequency, but rather before or after resonance, depending on the rate and direction of the excitation's frequency sweep. Also, it was noted that the system has a larger bandwidth and experiences a beat-like

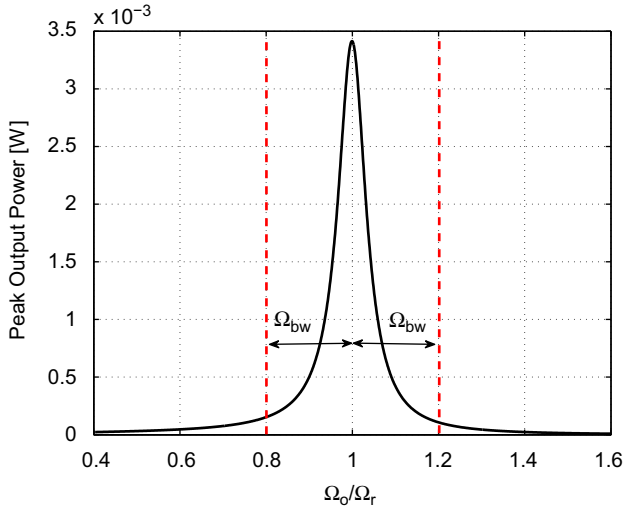

Fig. 2. Frequency response curve for the fixed-frequency case given by Eq. (15).

Table 1
Numerical values for PZT harvester.

Parameter (Symbol)	Value
Proof mass (M)	0.01 kg
Piezoelectric layer mass (M_p)	0.75 g
PZT layer modulus of elasticity (E_p)	66×10^9 N/m^2
PZT layer cross-sectional area (A_p)	1 cm^2
PZT layer thickness (t_p)	1 cm
Piezoelectric constant (e)	-14 C/m^2
PZT layer permittivity (ε)	1.137×10^{-8} F/m
Mechanical damping ratio (ζ)	0.01
Excitation amplitude (F)	1 N
Equivalent electric load (R_{eq})	100 kΩ

response shortly after the resonant frequency [23–28]. Henson [29] studied the response of several oscillatory systems to excitations with a harmonically varying frequency and noted that the system's natural frequency does not even need to be within the range of the excitation for its effects to be experienced. Such findings reveal that the transduction of energy harvesters in time-varying frequency environments are vastly different from their steady-state performance characteristics.

Finding an analytical solution becomes even more imperative when one realizes that numerical integration of the equations of motion for time-varying frequencies is very time-consuming and does not always provide the necessary insight for design and optimization especially given that variations in the excitation frequency can *stiffen* the problem numerically, making the integration harder for faster sweep rates and requiring even smaller integration time steps to adequately resolve each oscillation cycle. To resolve this issue, we use a mathematical identity that is frequently utilized in wave physics and signal processing. The identity known as the Jacobi–Anger's expansion [30] transforms the sine and cosine terms in the following form:

$$\cos(x\sin\varphi)=\sum_{k=-\infty}^{\infty}J_k(x)\cos(k\varphi), \tag{16a}$$

$$\sin(x\sin\varphi)=\sum_{k=-\infty}^{\infty}J_k(x)\sin(k\varphi), \tag{16b}$$

where $J_k(x)$ is the Bessel function of the first kind and order k.[2] Using Eqs. (16a) and (16b), the sine and cosine arguments in Eq. (5a) can be rewritten as

$$\cos[\Omega_o\tau+b\sin(\Omega\tau)]=\sum_{k=-\infty}^{\infty}J_k(b)\cos(\Omega_k\tau), \tag{17}$$

where $\Omega_k=\Omega_o+k\Omega$. Eq. (17) states that an excitation with sinusoidally varying frequency can be represented by a sum of infinite fixed-frequency excitations of different weights. Substituting Eq. (17) into Eq. (5a) yields

$$\ddot{\overline{x}}+2\zeta\dot{\overline{x}}+\overline{x}-\Theta\overline{V}=\sum_{k=-\infty}^{\infty}J_k(b)\cos(\Omega_k\tau). \tag{18}$$

In solving Eqs. (5a) and (5b), we use the principle of superposition and rewrite the governing equations in the form

$$\ddot{\overline{x}}_k+2\zeta\dot{\overline{x}}_k+\overline{x}_k-\Theta\overline{V}_k=\cos(\Omega_k\tau), \tag{19a}$$

$$\dot{\overline{x}}_k+\dot{\overline{V}}_k+\Gamma\overline{V}_k=0,\quad k=-\infty,\ldots,-1,0,1,\ldots,\infty, \tag{19b}$$

where

$$x_k=\frac{F_0J_k(b)}{K}\overline{x}_k=X_k\overline{x}_k,\quad V_k=\frac{\theta X_k}{C_p}\overline{V}_k, \tag{20}$$

and

$$\overline{x}=\sum_{k=-\infty}^{\infty}\overline{x}_k,\quad \overline{V}=\sum_{k=-\infty}^{\infty}\overline{V}_k. \tag{21}$$

[2] See Appendix A for a brief description of $J_k(x)$ and its relevant properties.

Noting that Eqs. (19a) and (19b) are similar to those associated with the fixed-frequency but with excitation frequency Ω_k instead of Ω_o, we can write the steady-state solution for each pair $\overline{x}_k(\tau)$ and $\overline{V}_k(\tau)$ as

$$\overline{x}_k(\tau) = \sqrt{A_k^2 + B_k^2}\sin\left[\Omega_k\tau + \arctan\left(\frac{A_k}{B_k}\right)\right], \tag{22}$$

$$\overline{V}_k(\tau) = \sqrt{C_k^2 + D_k^2}\sin\left[\Omega_k\tau + \arctan\left(\frac{C_k}{D_k}\right)\right], \tag{23}$$

where $A_k = A(\Omega_k)$, $B_k = B(\Omega_k)$, $C_k = C(\Omega_k)$, and $D_k = D(\Omega_k)$ are as defined in Eqs. (9)–(13).

3.1. Analytical expression for the average power

The solution obtained for the output voltage can be used to obtain an analytical expression for the average power which will aid in understanding the effect of the frequency parameters on the performance of the harvester. Such understanding will be very hard to attain by integrating the equations of motion for a large set of parameters. Since $V(\tau)$ is now given by an infinite sum, the average power can be obtained using

$$P_{\text{avg}} = \frac{\overline{V}_{\text{rms}}^2 V_{\text{oc}}^2}{R_{\text{eq}}}, \tag{24}$$

where $\overline{V}_{\text{rms}}$ is the root-mean-square (RMS) voltage. We expand Eq. (21) in the form

$$\overline{V} = \sum_{k=-\infty}^{\infty} (C_k\cos(\Omega_k\tau) + D_k\sin(\Omega_k\tau))J_k(b), \tag{25}$$

then apply Parseval's formula, [31], to Eq. (25), and obtain $\overline{V}_{\text{rms}}$ as

$$\overline{V}_{\text{rms}}^2 = \frac{1}{2}\sum_{k=-\infty}^{\infty} (C_k^2 + D_k^2)J_k^2(b) = \frac{1}{2}\sum_{k=-\infty}^{\infty} \frac{\Omega_k^2 J_k^2(b)}{E_k}, \tag{26}$$

where $E_k = E(\Omega_k)$ and $E(\Omega_k)$ is defined in Eq. (13). The average output power can also be expressed in the more insightful form:

$$P_{\text{avg}} = \frac{1}{2}\frac{V_{\text{oc}}^2}{R_{\text{eq}}}\sum_{k=-\infty}^{\infty} \overline{V}_p^2(\Omega_k)J_k^2(b) = \frac{1}{2}\sum_{k=-\infty}^{\infty} P_p(\Omega_k)J_k^2(b), \tag{27}$$

where $\overline{V}_p(\Omega_k)$ is the voltage amplitude for the fixed-frequency case and $P_p(\Omega_k)$ is the corresponding power.

In essence, Eq. (27) states that the average output power under a sinusoidally varying frequency can be obtained by calculating the average output power of the fixed-frequency, which is half of its magnitude, at a discrete albeit infinite set of frequencies separated by a constant frequency interval and adding them up with the square of the Bessel functions as weights. As depicted in Fig. 3, one can think of this as a *sampling* process in which the average power of the fixed-frequency

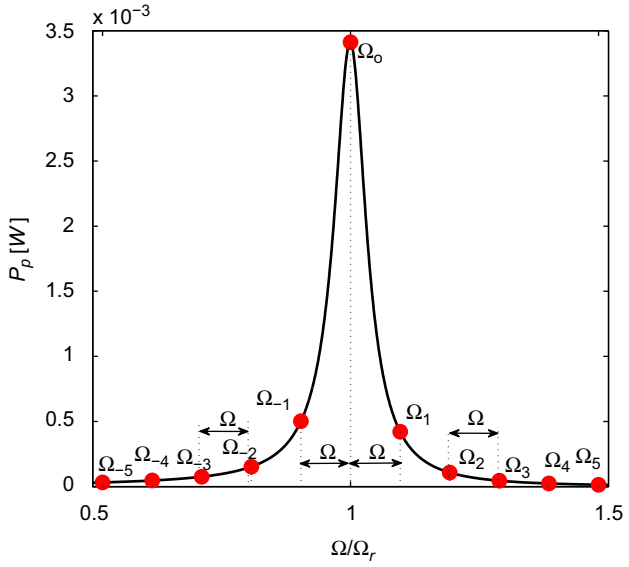

Fig. 3. Illustration of the process of "sampling" the fixed-frequency response curve to obtain the average output power for the time-varying frequency excitation of Eq. (2). The sampling interval in this example is $\Omega = 0.1\Omega_r$ and the harvester is tuned at the center frequency, that is, $\Omega_o = \Omega_r$.

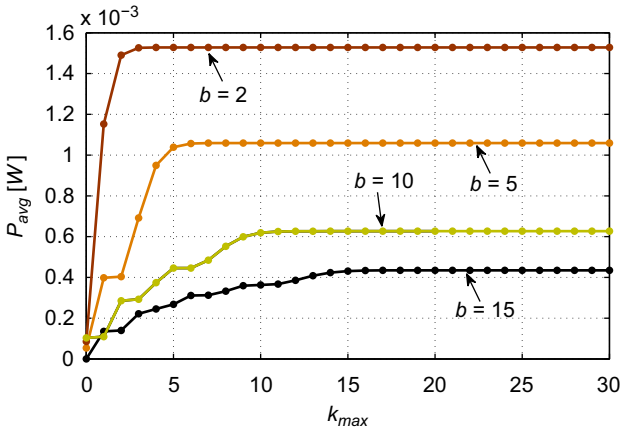

Fig. 4. Illustration of the convergence rate of the expression in Eq. (27). In this example, $\Omega_o = \Omega_r$ and $\Omega = 0.01\Omega_r$.

response is evaluated at discrete intervals, Ω, to either side of the center frequency, Ω_o, and each value is weighed by the Bessel function in the final sum. It is worth noting that Ω_o can be any frequency and not necessarily the resonance frequency as depicted in Fig. 3.

3.2. Convergence analysis

Although mathematically valid, the infinite sum in Eqs. (25) and (27) cannot be practically computed. Therefore, it is imperative to investigate the minimum number of terms that should be kept in the series for convergence. One realization that could assist in determining the convergence of the series is that the term $J_k(b)$ approaches zero rapidly when the order k gets larger than the argument, b, [29]. Indeed, the Bessel function $J_k(b)$ is practically zero when k is about two or three times the argument. As such, we can neglect any terms in Eq. (27) when $|k| > k_{\max}$, where we arbitrarily define $k_{\max}$ as three times the first integer larger than $|b|$. The curves in Fig. 4 demonstrate that this convergence criterion is conservative as convergence occurs when $k_{\max}$ is only slightly larger than b. This convergence criterion is followed in all simulations presented in this manuscript.

4. Frequency parameters analysis

Although the excitation frequency parameters are determined by the host structure and therefore are not controllable, we wish to study their effect on the output power in order to design harvesters that can harness energy efficiently from time-varying frequency excitations. Towards that end, we define a set of three parameters that hold a physical meaning to describe the excitation. The first parameter remains the *carrier* or *center* frequency, Ω_o. As discussed previously, it represents the center frequency around which the excitation frequency varies. We introduce a second parameter, σ, to describe the *range* of the excitation frequency. This constitutes a measure of the excitation's bandwidth around Ω_o. Using Eq. (3) for the instantaneous frequency, we can write

$$\sigma = b\omega \quad \text{or} \quad \overline{\sigma} = b\Omega, \tag{28}$$

where $\overline{\sigma}$ is the dimensionless version of σ and they are related through $\sigma = \omega_n\overline{\sigma}$.

The third and last parameter is the *sweep rate*, s, which is a measure of the frequency variation rate. Differentiating Eq. (3) with respect to time, we obtain

$$\dot{\Omega}_{\text{inst}}(t) = -s\sin(\omega t), \tag{29}$$

where the sweep rate, s, is given by

$$s = b\omega^2 \quad \text{or} \quad \overline{s} = b\Omega^2. \tag{30}$$

Here, $\overline{s}$ is the dimensionless version of s and they are related by $s = \omega_n^2\overline{s}$. In terms of σ and s, the modulation frequency and index can be written as

$$\omega = \frac{s}{\sigma} \quad \text{and} \quad b = \frac{\sigma^2}{s}. \tag{31}$$

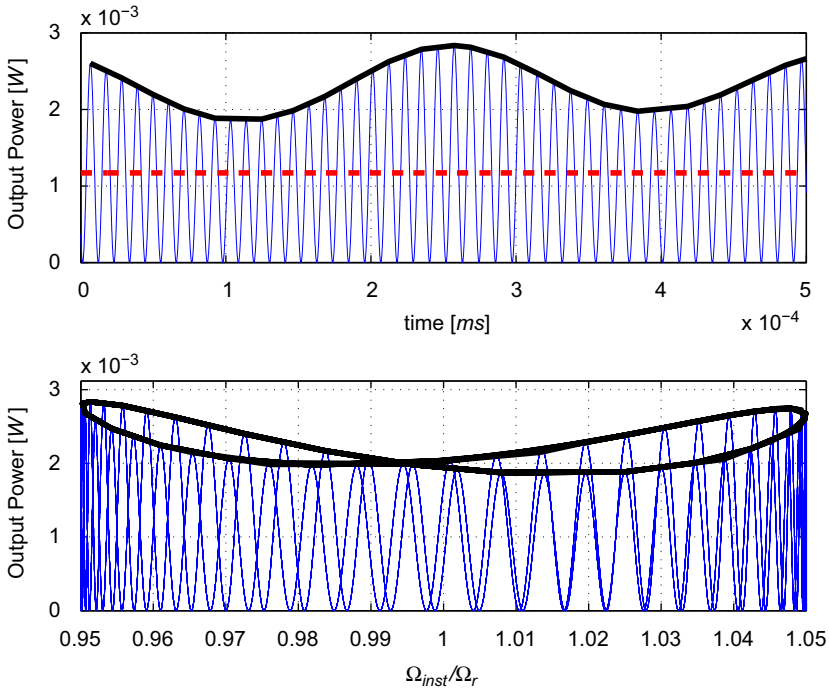

Fig. 5. Time history of the output power and instantaneous frequency response curve for $\overline{\sigma} = 0.05\Omega_r$, $\overline{s} = 0.002\Omega_r^2$ and $\Omega_o = \Omega_r$. The constant line represents the average power output, $P_{\text{avg}} = 1.1711$ mW.

4.1. Effect of frequency range on the output power

First, we study the effect of the range, σ, on the output power. We fix the sweep rate at $\overline{s} = 0.002\Omega_r$ and study variations of the output power with time and the instantaneous frequency for different values of the range, namely, $\overline{\sigma} = 0.05\Omega_r$, $0.1\Omega_r$, $0.2\Omega_r$ and $0.4\Omega_r$. In all cases, the harvester is tuned at the carrier frequency, that is, $\Omega_o = \Omega_r$. The results are displayed in Figs. 5–8.

We first note that the power envelop obtained using the analytical solution is in perfect agreement with the numerical integration which validates the Bessel's function approach. When the range increases, meaning the excitation frequency travels farther away from the center frequency in each direction, the valleys where the instantaneous power output is low become more pronounced (deeper) and last for longer periods of time, Figs. 5–8. This is expected because when the range increases, the excitation frequency spends longer periods of time away from resonance. Consequently, the resulting average power as predict via Eq. (27) and shown as a constant line in the figures decreases.

As the range increases, the instantaneous power envelopes also vary significantly. We observe that the value of the power at resonance and at the turning-point frequencies changes considerably when the range is increased from $0.05\Omega_r$ to $0.2\Omega_r$. However, beyond a certain threshold, the range has very little effect on the instantaneous power other than extending it to a wider range of frequencies. For the case considered here, $\overline{\sigma} = 0.2\Omega_r$ seems to be the threshold value beyond which any effect of the range on the center portion of the power frequency curve is negligible. Fig. 2 reveals that this value is representative of the bandwidth of the fixed-frequency response curve, leading to the conclusion that if the range is large enough to cover the whole bandwidth of the harvester, then any further effects of the range on the instantaneous power can be neglected.

4.2. Effect of sweep rate on the average power

To further understand the effect of the sweep rate, we use Eq. (27) to study variation of the average output power with the sweep rate for a fixed range of $\overline{\sigma} = 0.4\Omega_r$, since, as discussed previously, at this value any effect of the range selection on the instantaneous power is minimal. The results are displayed in Figs. 9(a) and (b) for two different cases, one in which the harvester is tuned at the center frequency and the other in which it is tuned at $\Omega_o = 1.3\Omega_r$.[3]

Examining Figs. 9(a) and (b), we note that the average power exhibits a complex variation with the sweep rate. We observe that the average power is initially constant. Subsequently, beyond $\overline{s} = 0.01\Omega_r^2$, the amplitude of the average power

[3] Such figures are very hard to obtain numerically especially at high sweep rates because the problem becomes very stiff numerically.

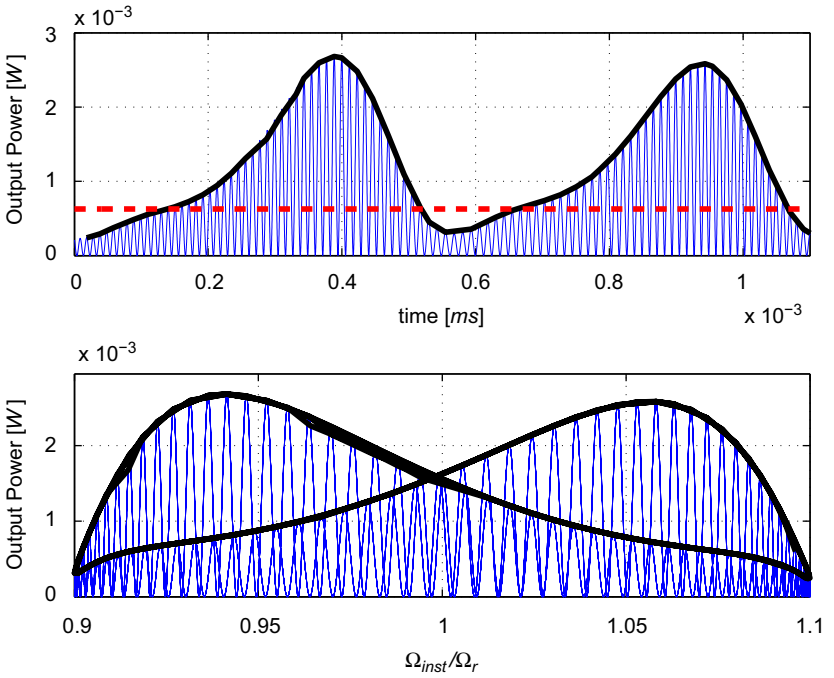

Fig. 6. Time history of the output power and instantaneous frequency response curve for $\overline{\sigma}=0.1\Omega_r$, $\overline{s}=0.002\Omega_r^2$ and $\Omega_o=\Omega_r$. The constant line represents the average power output, $P_{\text{avg}}=0.6267$ mW.

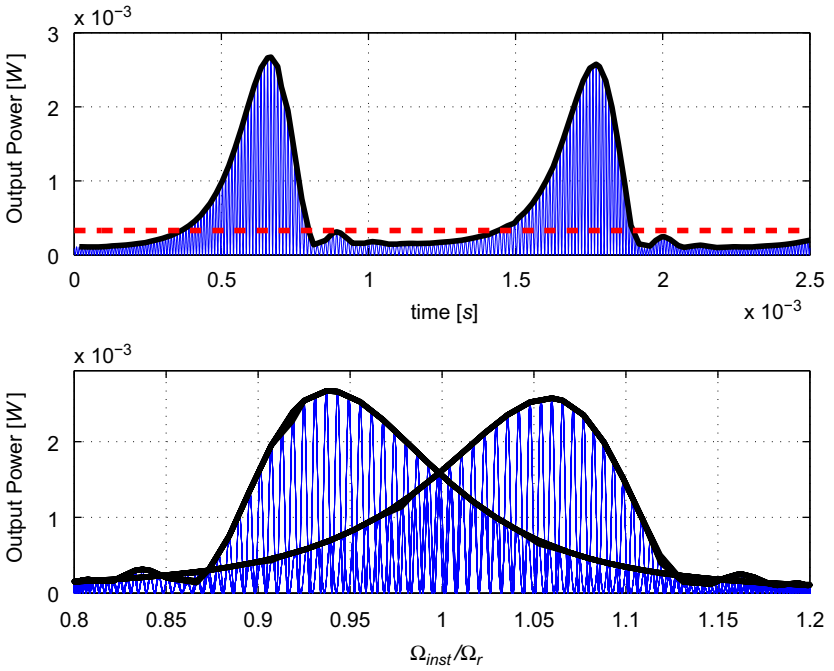

Fig. 7. Time history of the output power and instantaneous frequency response curve for $\overline{\sigma}=0.2\Omega_r$, $\overline{s}=0.002\Omega_r^2$ and $\Omega_o=\Omega_r$. The constant line represents the average power output $P_{\text{avg}}=0.3311$ mW.

starts to vary significantly, presenting a series of maxima and minima. As the sweep rate increases further, the average power approaches an asymptotic limit of $(1/2)P_p(\Omega_o)$. This limit which is represented by dashed lines in the figure represents the average power produced by the same harvester under a fixed-frequency excitation equal to the center frequency Ω_o.

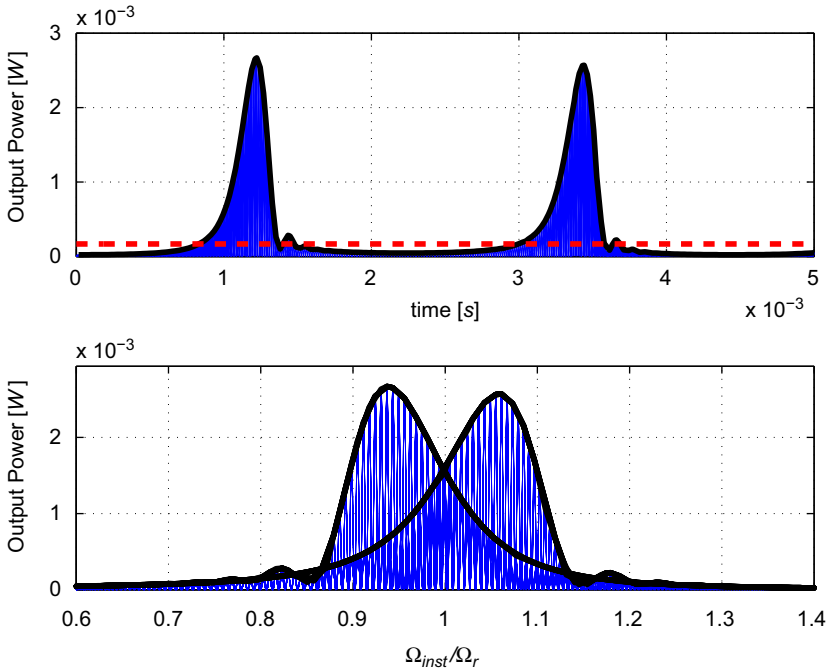

Fig. 8. Time history of the output power and instantaneous frequency response curve for $\overline{\sigma} = 0.4\Omega_r$, $\overline{s} = 0.002\Omega_r^2$ and $\Omega_o = \Omega_r$. The constant line represents the average power output $P_{avg} = 0.1685$ mW.

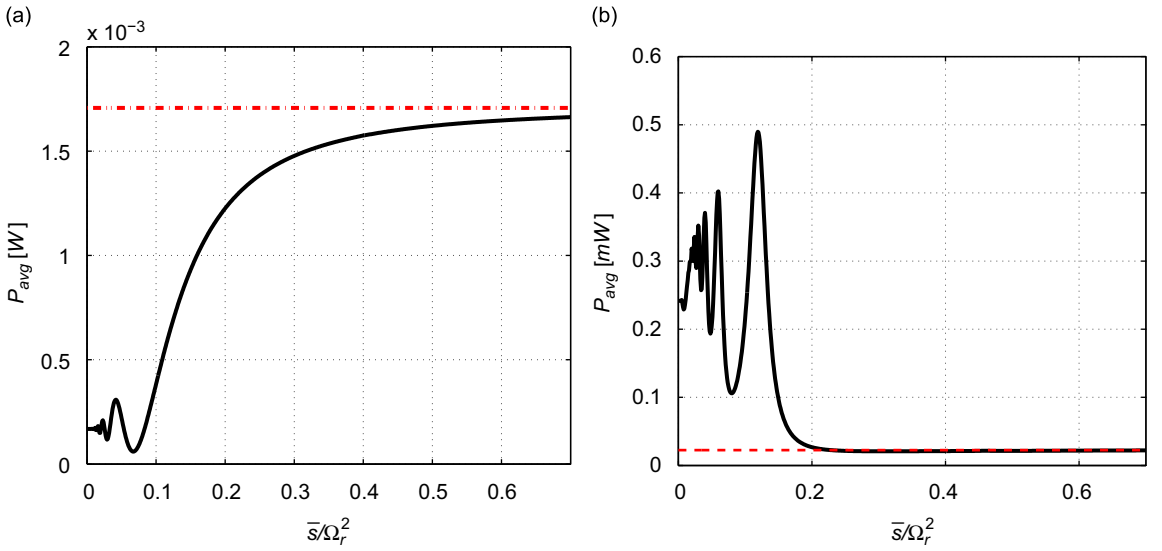

Fig. 9. Average output power for varying sweep rates for and (a) $\Omega_o = \Omega_r$, (b) $\Omega_o = 1.3\Omega_r$. In each case, the range is chosen as $\overline{\sigma} = 0.4\Omega_r$ and the constant horizontal lines represent the value of $(1/2)P_p(\Omega_o)$.

To understand this complex behavior of the power, we divide the analysis into three parts. The first deals with estimating the average power at low sweep rates, the second deals with moderate sweep rates, and the third deals with the analysis at high sweep rates.

4.2.1. Average power for low sweep rates

We consider four different values of the sweep rate, namely $\overline{s} = 0.001\Omega_r^2$, $\overline{s} = 0.002\Omega_r^2$, $\overline{s} = 0.004\Omega_r^2$, and $\overline{s} = 0.008\Omega_r^2$. We further note that the second case, $\overline{s} = 0.002\Omega_r^2$, is the same one depicted in Fig. 8, and hence, will not be repeated. The remaining results are displayed in Figs. 10–12, where both the power time history and the instantaneous power-frequency response of the harvester are depicted.

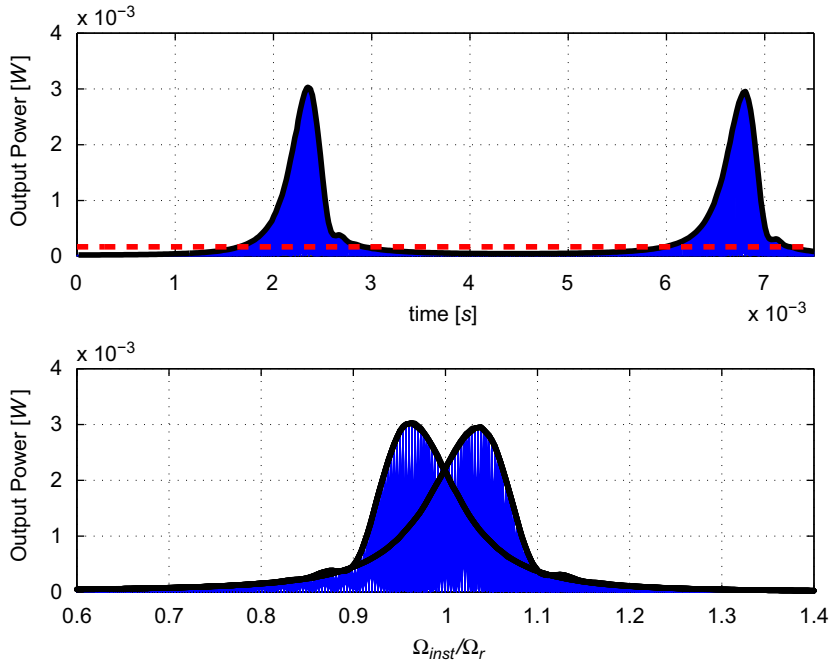

Fig. 10. Output power time history and instantaneous frequency response for $\overline{s}=0.001\Omega_r^2$, $\overline{\sigma}=0.4\Omega_r$ and $\Omega_o=\Omega_r$. The constant line represents the average power output of 0.1685 mW.

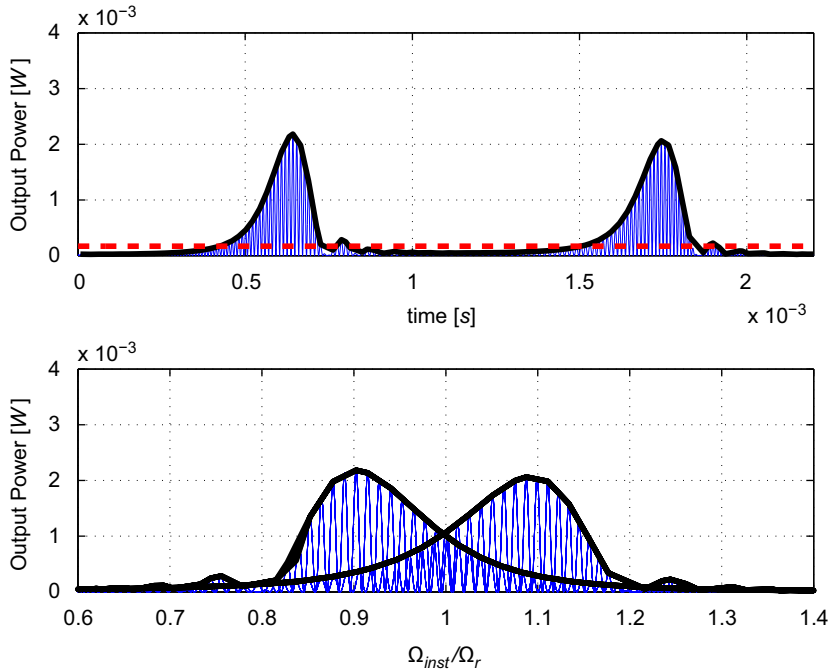

Fig. 11. Output power time history and instantaneous frequency response for $\overline{s}=0.004\Omega_r^2$, $\overline{\sigma}=0.4\Omega_r$ and $\Omega_o=\Omega_r$. The constant line represents the average power output of 0.1685 mW.

For the range of sweep rate considered in Figs. 10–12, which we consider as a slow sweep, it appears that the sweep rate has two opposite and offsetting effects on the average power. When the sweep rate increases, the instantaneous peak power decreases but the harvester's bandwidth increases causing the average power to remain almost constant. This opposite and offsetting effect can also be seen in the instantaneous frequency response curves shown in Figs. 8–12. As the

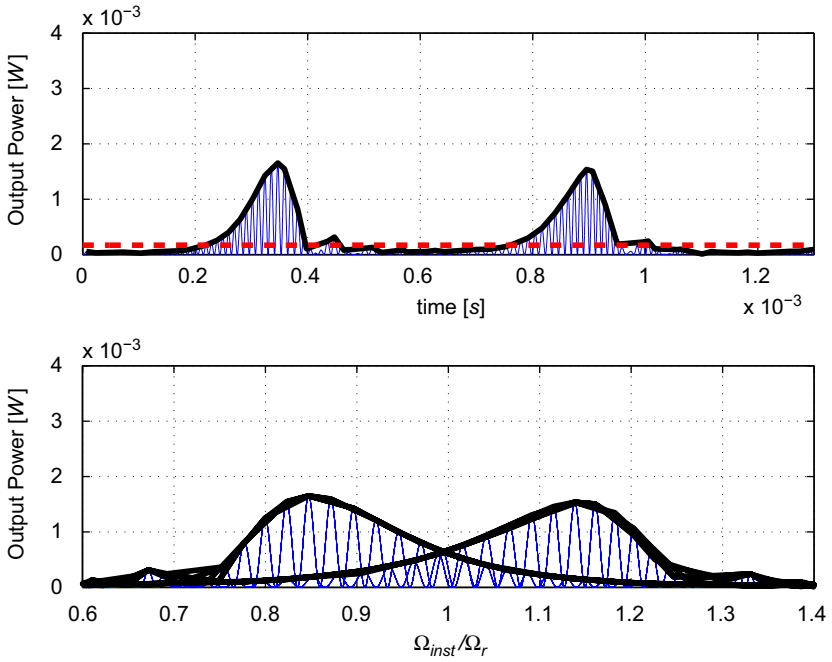

Fig. 12. Output power time history and instantaneous frequency response for $\bar{s} = 0.008\Omega_r^2$, $\bar{\sigma} = 0.4\Omega_r$ and $\Omega_o = \Omega_r$. The constant line represents the average power output of 0.1691 mW.

sweep rate increases, we see that the two peaks in the envelope become lower, leading to smaller power averages. At the same time, however, the bandwidth of frequencies wherein the amount of power is measurable becomes larger resulting in an increase in the power average. It is also worth mentioning that for the higher sweep rates, the power experiences a beat-like response shortly after the resonant frequency. This behavior is attributed to the ratio between the characteristic sweeping time which is related to $\bar{s}$ and the natural period of oscillation. When $\bar{s}$ is large, the system does not have enough time to build its steady-state response and the decay of the free response from the peak (governed by the natural period) interferes with the excitation frequency producing a beat-like response following the peak amplitude. This beat-like response may actually enhance the average power.

It is also evident that the response envelope exhibits two peaks: one occurs when Ω_{inst} is increasing which leads to a peak *after* resonance and the other occurs when Ω_{inst} is decreasing which leads to the peak *before* resonance. The system inertia separates the two peaks in the power envelope as the sweep rate increases. Because of its inertia, the harvester does not respond instantly to the excitation. During this time, the excitation frequency continues to change. The faster the sweep rate is, the farther away from resonance the instantaneous peak frequency will be.

4.2.2. Average power for moderate sweep rates

To understand the behavior of the average power for average sweep rates, the following two points need to be explained:

1. The average power in Fig. 9(b) varies about a higher mean, roughly $P_{\text{avg}} = 0.24$ mW when compared to that in Fig. 9(a), roughly 0.19 mW. This implies that, for average sweep rates, the harvester operates more efficiently when the carrier frequency Ω_o is not tuned at the resonance frequency.
2. The average power varies significantly with the sweep rate exhibiting a series of minima and maxima. This indicates that, the sweep rate has a considerable effect on the average power especially when the harvester is not tuned at the resonance frequency.

To explain the first of the preceding points, we refer to Figs. 13(a) and (b) where examples of the sampling process for each of the cases depicted in Fig. 9 are illustrated. When $\Omega_o = 1.3\Omega_r$, as shown in Fig. 13(b), the harvester's resonance frequency is very close to the end of the range of the excitation frequency. Near the end of the range, the rate of change of the instantaneous frequency, given by Eq. (29), is much lower because the excitation is near the turning point. As a result, the excitation frequency spends a longer period of time near the peak frequency when compared to the case at which $\Omega_o = \Omega_r$. This has the effect of increasing the output power considerably.

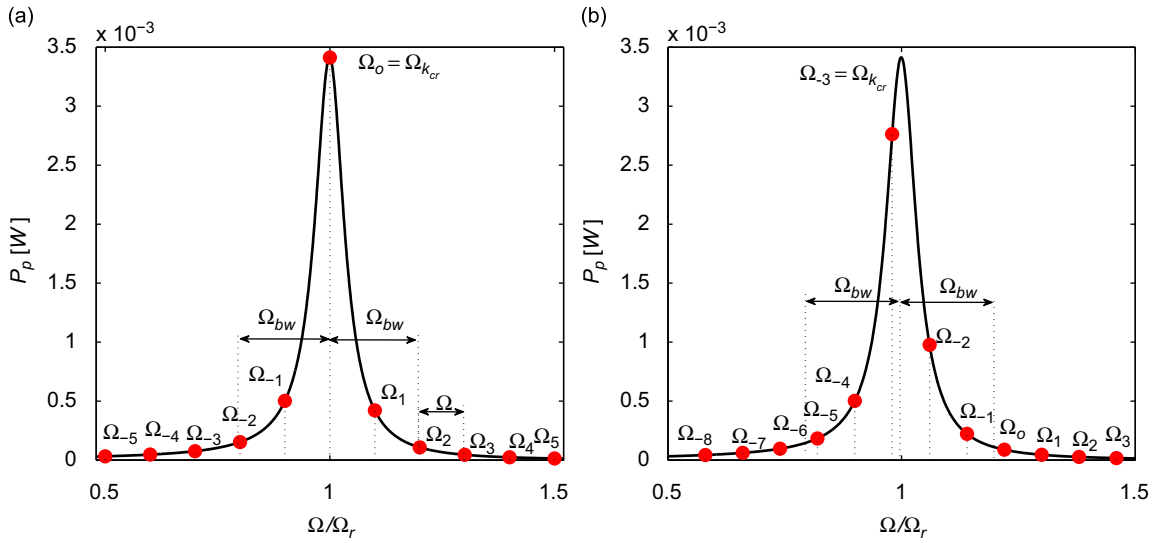

Fig. 13. Examples of the "sampling" process for (a) the harvester tuned at Ω_o and a sampling interval of $\Omega = 0.1\Omega_r$ and (b) the harvester off-center at $\Omega_o = 1.3\Omega_r$ and a sampling interval of $\Omega = 0.08\Omega_r$. In the first case, k_{cr} is always 0 and the peak is always part of the sampling process. If the harvester is off-center, though, the resonance may not be part of the sampling process as seen in (b), where $k_{cr} = -3$. In both examples, there are five terms within the harvester bandwidth.

To explain the second point, we expand Eq. (27) in terms of the amplitude of the output power in the fixed frequency case to obtain

$$P_{avg} = \tfrac{1}{2}[\cdots + P_p(\Omega_{-1})J_{-1}^2(b) + P_p(\Omega_o)J_0^2(b) + P_p(\Omega_1)J_1^2(b) + \cdots]. \tag{32}$$

This equation clearly indicates that the average power for the varying frequency case is obtained by "sampling" the fixed-frequency response curve, Fig. 2, at a constant frequency interval given by the Ω_k' s. To guarantee convergence, the preceding expression has to be truncated at $k = b$ as discussed in Section 3.2. By inspecting Eq. (32), we note the following:

- For low sweep rates, the frequency interval of the sampling process, Ω, is very small. As such, a large number of Ω_k fall within the harvester bandwidth and more terms should be kept to guarantee the convergence of the series in Eq. (32).
- The Bessel functions have a large argument and in that case, also see Appendix A, the need for keeping more terms for the convergence of the series in Eq. (32) is reinforced.
- The only frequency which is always part of the sampling process is the center frequency Ω_o. Therefore, tuning the harvester resonance frequency to Ω_o as in the case of Figs. 9(a) and 13(a) is the only way to guarantee that the resonance peak is part of the sampling process independent of the sampling interval. If the center frequency of the excitation is not tuned at the resonance frequency of the harvester, the resonance peak may not be a part of the sampling process which can considerably lower the average output power.

When the harvester is not tuned at the center frequency, as shown in Fig. 9(b), variation in the average power can be understood as a result of the sampling processes which is affected by the sweep rate. Specifically, when the sweep rate yields a sampling process that includes the resonance frequency, the average power exhibits a maximum. On the other hand, when the resonance frequency is not included in the process and all the sampling Ω_k' s are far from Ω_r, the average power exhibits a minimum. To reinforce this finding, two excitation frequencies with the same center frequency are considered as shown in Fig. 14. The first of which has a sweep rate of $\bar{s} = 0.06\Omega_r^2$ and corresponds to a peak in the average power curve seen in Fig. 9(b). In this case, the resonance frequency Ω_r coincides with Ω_{-2} and the resonance is included in the sampling process. In the second case, as shown in Fig. 14(b), the sweep rate $\bar{s} = 0.08\Omega_r^2$ yields a sampling process where the resonance frequency falls exactly halfway between the nearest sampled frequencies. This yields a minimum in the average power curve shown in Fig. 9(b).

For further confirmation of these conclusions, the values of $\bar{s}$ at which some of the maxima and minima seen in Fig. 9(b) occur are tabulated in Table 2, together with the equivalent sampling frequency interval and some of the sampling frequencies around Ω_r. In accordance with the previous discussion, the maxima occur when Ω_r is part of the sampling process ($\Omega_r \approx \Omega_{-1}$ for the first peak listed in Table 2 and $\Omega_r \approx \Omega_{-2}$ for the second) and the minima occur when Ω_r is the average of the two closest Ω_k' s (for the first minimum listed in Table 2, $\Omega_r \approx (\Omega_{-1} + \Omega_{-2})/2$ and, for the second minimum, $\Omega_r \approx (\Omega_{-2} + \Omega_{-3})2$).

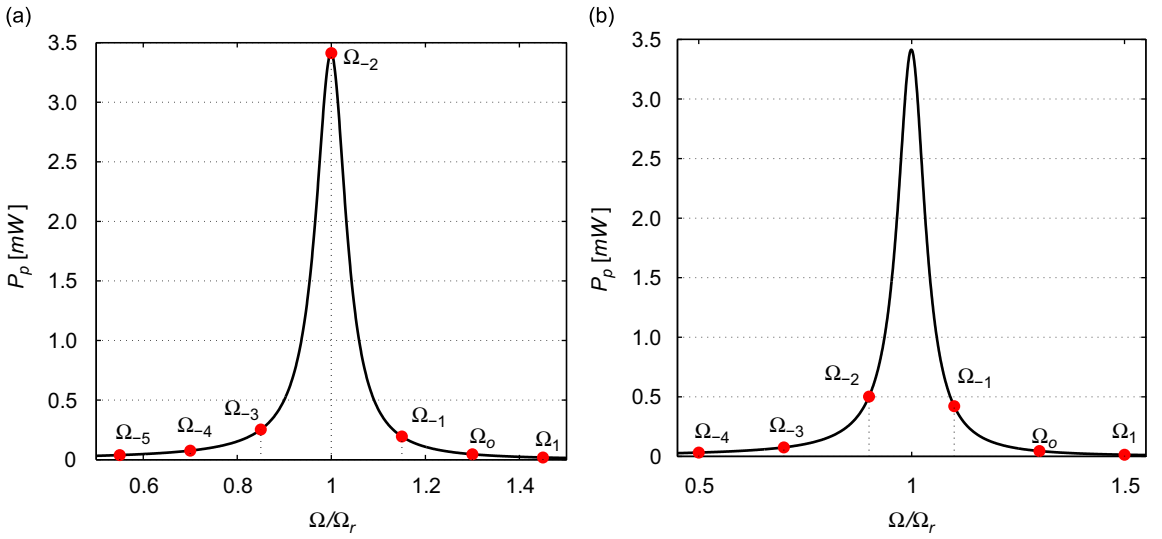

Fig. 14. Illustration of the sampling process where $\Omega_o = 1.3\Omega_r$ and $\overline{\sigma} = 0.4\Omega_r$. (a) $\Omega = 0.15\Omega_r$ ($\overline{s} = 0.06\Omega_r^2$) and the resonance frequency is included in the sampling process; this leads to a maximum in Fig. 9(b). (b) $\Omega = 0.2\Omega_r$ ($\overline{s} = 0.08\Omega_r^2$) and the resonance frequency is excluded from the sampling process, leading to a minimum in Fig. 9(b).

Table 2
Frequency parameters and resulting sampling frequencies at some of the maxima and minima seen in Fig. 9(b).

Minima			**Maxima**		
$\frac{\overline{s}}{\Omega_r^2}$	$\frac{\Omega}{\Omega_r}$	$\frac{(\Omega_{-3},\Omega_{-2},\Omega_{-1})}{\Omega_r}$	$\frac{\overline{s}}{\Omega_r^2}$	$\frac{\Omega}{\Omega_r}$	$\frac{(\Omega_{-2},\Omega_{-1},\Omega_o)}{\Omega_r}$
0.080	0.2	(0.7,0.9,1.1)	0.119	0.2975	(0.705,1.0025,1.3)
0.048	0.12	(0.94,1.06,1.18)	0.06	0.15	(1.0,1.15,1.3)

In conclusion, when the harvester's resonance frequency is not tuned at the center frequency of the excitation, we can infer the following:

1. A maximum in P_{avg} occurs when the values of Ω_o, $\overline{s}$ and $\overline{\sigma}$ yield a sampling process in which resonance is included, that is, when $\Omega_r = \Omega_k$ for any k.
2. A minimum in P_{avg} occurs when the values of Ω_o, $\overline{s}$ and $\overline{\sigma}$ yield a sampling process in which resonance is as far from the nearest Ω_k as possible. Since the sampling interval is constant, this happens whenever resonance is equidistant from the two nearest Ω_k' s at either side. That is, whenever Ω_r is the average between the two nearest Ω_k' s.

When the harvester is tuned at Ω_o as shown in Figs. 9(a) and 13(a), resonance is always a part of the sampling process, independent of the values of $\overline{s}$ and $\overline{\sigma}$. As such, the previous explanation of the oscillations at low sweep rates is not sufficient. Referring to Eq. (32), we note that although the power at resonance is now always included in the series, its associated weighting, $J_0^2(b)$, varies with the argument of the Bessel function. Hence, the power at resonance may be very small if the associated weight $J_0^2(b)$ is small. Conversely, the larger $J_0^2(b)$ is, the larger is the influence of resonance on the resulting average power. By virtue of this understanding, one can expect the peaks seen in Fig. 9(a) to correspond to maxima in $J_0^2(b)$, and the valleys to correspond to minima in $J_0^2(b)$. Inspecting Fig. 15(a), we can see that indeed the peaks in P_{avg} and $J_0^2(b)$ occur at the same time (The reader has to bear in mind that the approximate curve shown in Fig. 15(a) is proportional to $J_0^2(b)$).

Values of $\overline{s}$ that yield some of the maxima and minima seen in Fig. 9(a) are tabulated together with the corresponding values of the modulation index, b, and the nearest zero or critical points of $J_0(x)$. Upon inspection of the results available in Table 3, the correlation between the values of b and the zeros of $J_0(b)$ for the minima, and between b and the critical points of $J_0(b)$ for the maxima, becomes evident.

It is worth noting that variations in the average power shown in Fig. 9(a) are more pronounced for larger values of the sweep rate. Recalling that higher values of $\overline{s}$ lead to both lower values of b and higher values of Ω, this behavior can be explained by

1. The minima occur when $J_0(b)$=0, in which case the resonance value does not appear in the expansion of Eq. (24). Therefore, the terms with the highest power left in the series are $P_p(\Omega_1)$ and $P_p(\Omega_{-1})$. The larger the sampling frequency is, the farther away from resonance these terms will be, making the minima even smaller.

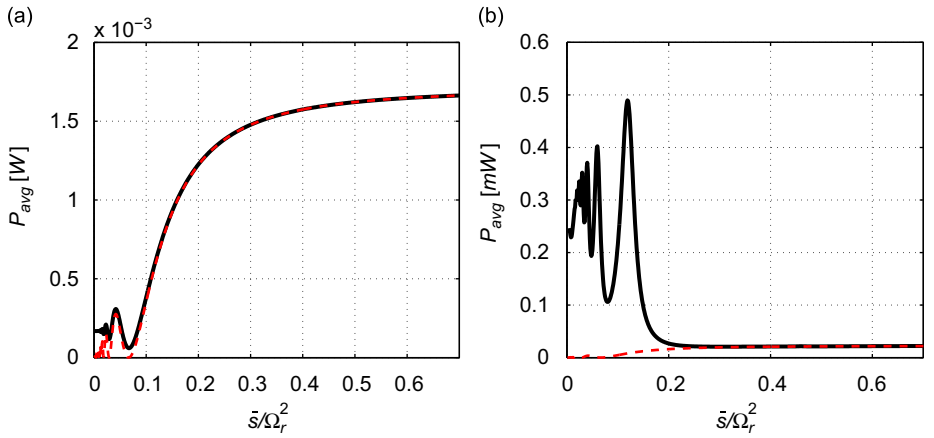

Fig. 15. Comparison of the results obtained using Eq. (32) and the single-term approximation in Eq. (33) for a harvester tuned at (a) Ω_o and (b) $\Omega_o = 1.3\Omega_r$.

Table 3
Minima and maxima seen in Fig. 9(a) and zeros and critical points of $J_o(x)$.

Minima			**Maxima**		
$\bar{s}$ $[\times\Omega_r^2]$	b	$J_o(x)=0$	$\bar{s}$ $[\times\Omega_r^2]$	b	$J_o'(x)=0$
0.067	2.3881	2.4048	0.042	3.8095	3.8317
0.029	5.5172	5.5201	0.023	6.9565	7.0156

2. The maxima occur when $J_0(b)$ is a maximum or minimum. As can be seen in Fig. 18 in Appendix A, when b increases, the magnitude of $J_0(b)$ at its infinitely critical points associated with $J_0'(b)=0$ decreases. As such, $J_0^2(b)$ is larger for lower values of b. This implies that the weight of resonance in P_{avg} is larger when b is smaller.

4.2.3. Average power for high sweep rates

Since for small arguments, all Bessel functions of the first kind are very small compared to $J_0(x)$, see Fig. 18, and given that as $\bar{s}$ increases, b decreases; we can neglect all the terms in the expansion of Eq. (32), except for the one associated with $J_0(x)$. This yields

$$P_{\text{avg}} = \frac{1}{2}\left[\cdots + P_p(\Omega_{-1})\underbrace{J_{-1}^2(b)}_{\approx 0} + P_p(\Omega_o)J_0^2(b) + P_p(\Omega_1)\underbrace{J_1^2(b)}_{\approx 0} + \cdots\right] \approx \frac{1}{2}P_p(\Omega_o)J_0^2(b), \tag{33}$$

which is an approximation only valid for very high sweep rates. Figs. 15(a) and (b) compare the full expression for P_{avg} in Eq. (32) and the single-term approximation presented in Eq. (33) demonstrating the excellent agreement between the curves for high sweep rates.

Now, since b approaches zero as $\bar{s}$ approaches infinity, and $J_0(b)$ approaches one as b approaches zero, we can write

$$P_{\text{avg}} \to \frac{1}{2}P_p(\Omega_o) \quad \text{as} \quad \bar{s} \to \infty. \tag{34}$$

In other words, as the sweep rate increases while the range is kept constant, the harvester behaves as if it was under a fixed-frequency excitation equal to the center frequency Ω_o. For the particular case shown in Fig. 9(a), we have $\Omega_o = \Omega_r$. Hence, the asymptotic value of P_{avg} is $(1/2)P_p(\Omega_r)$, which is the average power harvested at the resonance frequency. Since $\Omega_o = 1.3\Omega_r$ for the case illustrated in Fig. 9(b), the asymptotic average power approaches $(1/2)P_p(1.3\Omega_r)$. When compared to the first case, this is a small value because $\Omega_o = 1.3\Omega_r$ is outside the bandwidth of the fixed-frequency harvester as shown in Fig. 2. Physically, this implies that when the frequency variation happens at a very fast time scale, the harvester does not have enough time to responed to it and behaves as if it is being excited at the center frequency.

From the preceding discussion, we conclude that when the excitation has a very high sweep rate, the harvester should be tuned such that the carrier frequency Ω_o is equal to the resonance frequency Ω_r.

5. Optimal load

In their recent work, Renno et al. [32] studied the optimality of energy harvesters in the fixed frequency scenario. They found that, depending on the value of the mechanical damping ratio, there might exist more than one optimal electric load that maximize the output power. Specifically, they have shown that their exists a bifurcation damping ratio below which there are two optimal electric loads and beyond which there is only one optimal load. Here, we make use of Eq. (27) to elucidate how the optimal values of the electric load vary with the sweep rate of the excitation. Basically, we differentiate Eq. (27) with respect to the electric load, set the resulting equation equal to zero, and solve for the resulting optimal load numerically. The sign of the second derivative of Eq. (27) with respect to the load resistance is always checked to guarantee that the optimal load yields maximum power.

Based on the fixed-frequency analysis, we choose two values of the damping ratio, ζ; one below and one above the bifurcation value. Fig. 16(a) depicts variation of the optimal load with the sweep rate for ζ larger than the bifurcation damping ratio. It is shown that at low sweep rates, the optimal load is close to that obtained using the fixed-frequency analysis. However, as the sweep rate increases, the optimal load starts to vary around the fixed-frequency optimal value. On the other hand, when ζ is less than the bifurcation damping ratio, namely, $\zeta = 0.01$, the optimal load varies significantly between the two optimal values obtained for the fixed-frequency scenario.

These results can also be observed by inspecting variation of the power with the load for different values of the sweep rate as depicted in Figs. 17(a) and (b). When $\zeta = 0.07$, maxima in the average power do not vary significantly with variation in the sweep rate. On the other hand, when $\zeta = 0.01$ it is easily observable that the maxima alternate between being large and closer to the larger optimal value of the fixed frequency case and being small and closer to the lower optimal value.

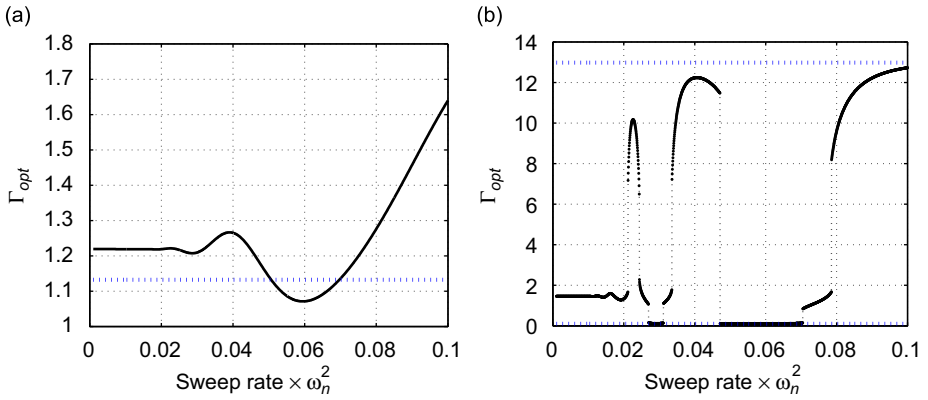

Fig. 16. Variations of the optimal load with the sweep rate for (a) $\zeta = 0.07$ and (b) $\zeta = 0.01$. Results are obtained for $\Theta = 0.26$ and $F_0 = 1$.

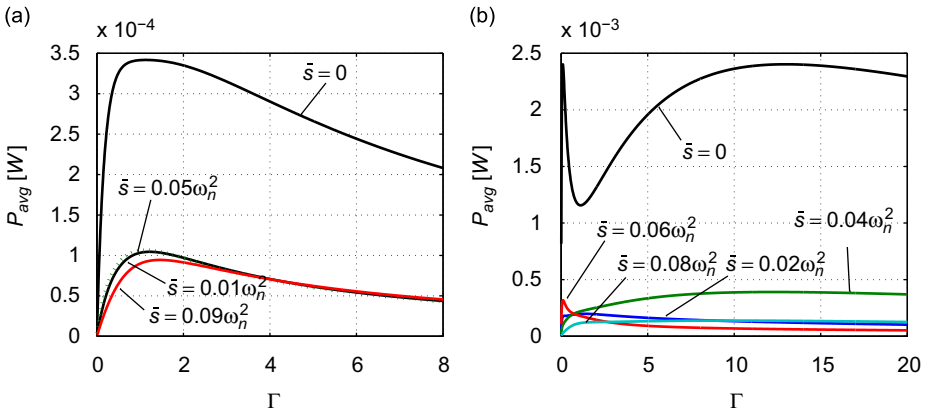

Fig. 17. Variations of the average power with the load for different sweep rates and for (a) $\zeta = 0.07$ and (b) $\zeta = 0.01$. Results are obtained for $\Theta = 0.26$ and $F_0 = 1$.

6. Tuning and design considerations

The results obtained in this manuscript can provide helpful information for tuning and designing harvesters subjected to sinusoidally varying frequency sources similar to the one considered herein. Specifically, given a host structure with an excitation described by the parameters Ω_o, Ω, and b, this study reveals some ideas for efficient tuning of the harvester.

One of the critical design consideration of the harvester is its resonance frequency, Ω_r. Obviously, for a fixed-frequency excitation, the harvester should be designed such that Ω_r matches the excitation frequency. In this case, however, the excitation does not posses a fixed well-defined frequency but one that spans a certain range. The results discussed in the previous section, expressed in Eq. (33), and shown in Fig. 9(a) suggest that, when the sweep rate of the excitation is very high, the harvester will extract the same amount of power that it can extract from a fixed-frequency excitation when tuned at resonance.

For lower and more realistic sweep rates, it is observed that the average power can be lower when the harvester's resonance frequency is tuned at Ω_o. This depends on the rate of change of the excitation frequency sweep. In the case of the sinusoidally varying frequency considered in this work, the rate of change is minimum near the end of the frequency range (turning points). If the turning point is chosen such that it coincides with the resonance frequency of the harvester, the average power can be increased significantly. Also, it is concluded that the sweep rate has a significant effect on the average output power. Therefore, the following few points should be emphasized in the design of the harvester:

- At low sweep rates, one can benefit from tuning the harvester at a position other than the center frequency. However, it is observed that when detuning the harvester from the center frequency, resonance may no longer be a part of the sampling process which could significantly lower the output power. Therefore, care must be taken so that this does not occur.
- At low sweep rates, the off-center harvester showed maxima in the average power whenever resonance was part of the sampling process, that is, $\Omega_r = \Omega_{k_{cr}}$ for some k_{cr}. As such, the first criterion for the choice of the harvester's resonance frequency is to satisfy the condition $\Omega_r = \Omega_o + k_{cr}\Omega$ for any integer k_{cr}.
- Since the fixed-frequency response curve is sampled with weights given by the square of the Bessel functions of the first kind, it is also desirable to maximize these weights for those sampling frequencies within the harvester bandwidth and closer to resonance. This is the condition that guides us in choosing k_{cr}.

As the excitation is symmetric about Ω_o, one viable alternative that might improve performance even further, is to use *two* similar harvesters tuned at either side of Ω_o. First, we decide on a position for Ω_r in accordance with the previously defined conditions, and then we place a second harvester with its natural frequency equidistant from Ω_o but at the other side of it. These are just suggestions based on the previous discussion and the performance of the harvester in each case has to be evaluated.

7. Conclusions

This effort marks a first attempt to theoretically analyze the response of energy harvesters to excitations having a time-varying frequency. Results provided a new perspective that cannot be attained using a traditional steady-state fixed-frequency analysis, thereby moving our understanding a step closer towards elucidating the transduction of energy harvesters in realistic environments. It is shown that the average output power of the harvester has a significant dependence on the sweep rate, center frequency, and range of the excitation. Specifically, we have shown that, for ranges that are less than the bandwidth of the fixed-frequency power curves, changing the range of the excitation has a considerable effect on the instantaneous output power. Furthermore, it is observed that the dependance of the average power on the sweep rate can be divided into three major categories. For low sweep rates, the average power remains constant. For moderate sweep rates, the average power shows significant dependance on the sweep rate with the average power curve exhibiting a series of maxima and minima. For such excitations, we have illustrated that one can benefit from tuning the excitation's center frequency outside the bandwidth of the steady-state fixed-frequency harvester and away from it resonance frequency. For high sweep rates, the average power approaches an asymptotic limit equal to the average power at the carrier frequency. Therefore, to maximize the average power in such cases, the harvester's resonance frequency should be tuned to the excitation's center frequency. Such results clearly demonstrate that one cannot solely depend on the steady-state characteristics of the fixed-frequency harvester for the design of efficient energy harvesters. More light should be shed on the response of energy harvesters to different types of environmental excitations.

Appendix A. Bessel function of the first kind

This appendix briefly discusses the Bessel functions of the first kind and integer order and summarizes their properties that are in some way pertinent to the present work. For further information about Bessel functions, we refer the reader to [31].

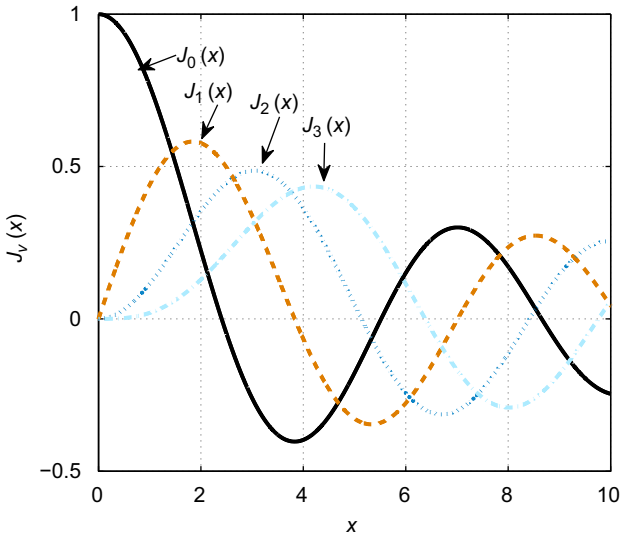

Fig. 18. First four Bessel functions. Note that as $x \to 0$, $J_0(x)$ is much larger than $J_1(x)$, $J_2(x)$ or $J_3(x)$.

Bessel functions of the first kind and positive integer order v are defined as

$$J_v(x) = \sum_{n=0}^{\infty} \frac{(-1)^n}{n!(n+v)!} \left(\frac{x}{2}\right)^{2n+v}, \tag{A.1}$$

$$J_{-v}(x) = (-1)^v J_v(x). \tag{A.2}$$

An important consequence of Eq. (A.2) is that

$$J_v^2(x) = J_{-v}^2(x), \tag{A.3}$$

which means that the weights of the sampling procedure are symmetric around the center frequency Ω_o.

Following are some of the important properties of the Bessel functions of the first kind. Fig. 18 depicts the first four of these functions which aid in understanding these properties.

1. $$J_v(0) = \begin{cases} 1 & \text{if} \quad v = 0, \\ 0 & \text{if} \quad v \neq 0. \end{cases} \tag{A.4}$$
2. For low values of x, $J_0(x) \gg J_{v\neq 0}(x)$. This leads to the conclusion that as $x \to 0$, $J^2_{v\neq 0}(x) \approx 0$. This result was utilized to obtain an approximation for the average power at high values of the sweep rate.
3. The magnitude of $J_v(x)$ decreases with both of the argument, x, and the order v. A characteristic that is critical toward understanding the behavior of the average power shown in Fig. 9.
4. $$J_0'(x) = -J_1(x). \tag{A.5}$$

References

[1] H. Sodano, D.J. Inman, G. Park, A review of power harvesting from vibration using piezoelectric materials, *The Shock and Vibration Digest* 36 (2004) 197–205.
[2] H. Sodano, D.J. Inman, G. Park, Generation and storage of electricity from power harvesting devices, *Journal of Intelligent Material Systems and Structures* 16 (2005) 67–75.
[3] S. Roundy, On the effectiveness of vibration-based energy harvesting, *Journal of Intelligent Materials and Structures* 16 (2005) 809–823.
[4] A.J. duPlessis, M.J. Huigsloot, F.D. Discenzo, Resonant packaged piezoelectric power harvester for machinery health monitoring, *Proceedings of Smart Structures and Materials Conference*, SPIE, San Diego, CA, 2005, p. 5762.
[5] D.J. Inman, B.L. Grisso, Towards autonomous sensing, *Proceedings of Smart Structures and Materials Conference*, SPIE, San Diego, CA, 2006, p. 61740T.
[6] R.S. Sanders, M.T. Lee, Implantable pacemakers, *Proceedings of the IEEE* 84 (3) (1995).
[7] I.D. Capel, H.M. Dorrell, E.P. Spencer, M.W. Davis, The amelioration of the suffering associated with spinal cord injury with subperception transcranial electrical stimulation, *Spinal Cord* 41 (2003) 109–117.
[8] S. Roundy, P.K. Wright, J. Rabaey, A study of low level vibrations as a power source for wireless sensor nodes, *Computer Communications* 26 (2003) 1131–1144.
[9] S. Roundy, P.K. Wright, A piezoelectric vibration-based generator for wireless electronics, *Journal of Intelligent Materials and Structures* 16 (2005) 809–823.

[10] S.W. Arms, C.P. Townsend, D.L. Churchill, G.H. Galbreath, S.W. Mundell, Power management for energy harvesting wireless sensors, *Proceedings of the Smart Structures and Materials Conference*, SPIE, San Diego, CA, 2005, pp. 5763, 267–275.
[11] J.A. Paradiso, T. Starner, Energy scavenging for mobile and wireless electronics, *IEEE Pervasive Computing* 4 (2005) 18–27.
[12] N. duToit, B. Wardle, Experimental verification of models for microfabricated piezoelectric energy harvesters, *AIAA Journal* 45 (2007) 1126–1137.
[13] A. Erturk, D. Inman, A distributed parameter electromechanical model for cantilevered piezoelectric energy harvesters, *Journal of Vibration and Acoustics, Transaction of ASME* 130 (2008) 1–14.
[14] S. Roundy, Y. Zhang, Toward self-tuning adaptive vibration-based micro-generators, *Smart Materials*, *Nano- and Micro-Smart Systems*, Sydney, Australia, 2005.
[15] N.G. Stephen, On energy harvesting from ambient vibration, *Journal of Sound and Vibration* 293 (2006) 409–425.
[16] J. Renno, M.F. Daqaq, J. Farmer, D.J. Inman, Parameter optimization of a vibration-based energy harvester, *Proceedings of the ASME International Design and Engineering Technical Conference*, IDETC2007, Las Vegas, NV, 2007.
[17] T. Osorio, M.F. Daqaq, Effect of bias conditions on the optimal energy harvesting using magnetostrictive materials, *Proceedings of the SPIE*, San Diego, CA, 2008, p. 69280B.
[18] D. Lee, Wireless and powerless sensing node system developed for monitoring motors, *Sensors* 8 (2008) 5005–5022.
[19] A. Erturk, D.J. Inman, An experimentally validated bimorph cantilever model for piezoelectric energy harvesting from base excitations, *Smart Materials and Structures* 18 (2009) 025009.
[20] T.H. Ng, W.H. Liao, Sensitivity analysis and energy harvesting for a self-powered piezoelectric sensor, *Journal of Intelligent Materials and Structures* 16 (1995) 785–797.
[21] T. Osorio, M.F. Daqaq, On the reduced-order modeling of energy harvesters, *Journal of Intelligent Materials and Structures* 20 (2009).
[22] F.M. Lewis, Vibration during acceleration through a critical speed, *Transactions of the American Society of Mechanical Engineers* 54 (1932) 253–261.
[23] D.L. Cronin, Response of Linear Viscous-damped Systems to Excitations having Time-varying Frequency, Ph.D. Thesis, California Institute of Technology, Pasadena, CA, 1966.
[24] G. Hok, Response of linear resonant systems to excitation of a frequency varying with time, *Journal of Applied Physics* 19 (1948) 354–361.
[25] A.V. Parker, The Response of a Vibrating System to Several Time-dependent Frequency Excitations, Master's Thesis, Iowa State University, Ames, IA, 1962.
[26] G.D. McCann, R.R. Benett, Vibration of multifrequency systems during acceleration through critical speeds, *Journal of Applied Mechanics* 16 (1949) 375–382.
[27] R. Markert, M. Seidler, Analytically based estimation of the maximum amplitude during passage through resonance, *International Journal of Solids and Structures* 38 (2001) 1975–1992.
[28] S. Zhou, J. Shi, The analytical imbalance response of Jeffcott rotor during acceleration, *Journal of Manufacturing Science and Engineering* 123 (2001) 299–302.
[29] R. Henson, Response of an oscillating system to harmonic forces of time-varying frequency, *AIAA Journal* 46 (8) (2008).
[30] C.D. Cantrell, *Modern Mathematical Methods for Physicists and Engineers*, Cambridge University Press, New York, 2000.
[31] A. Broman, *Introduction to Partial Differential Equations: From Fourier Series to Boundary-value Problems*, Addison-Wesley, Great Britain, 1970.
[32] J.M. Renno, M.F. Daqaq, D.J. Inman, On the optimal energy harvesting from a vibration source, *Journal of Sound and Vibration* 320 (2009) 386–405.